Mechanical and Physical Properties – A Way to assess quality of Laser Sintered Parts

S. Rüsenberg, L. Schmidt, and H.-J. Schmid

Direct Manufacturing Research Center, University of Paderborn, Paderborn, Germany
E-Mail: stefan.ruesenberg@upb.de; hans-joachim.schmid@upb.de

REVIEWED, August 17 2011

Abstract

The aim of this paper is the description and evaluation of physical properties like porosity and density and their influence on mechanical properties of laser sintered polyamide parts. For example, by reducing the porosity an increase of mechanical properties is possible. The correlation of laser parameters to these properties is investigated in detail. The energy density is an important parameter for the laser sintering process. By changing laser power, scan velocity and hatch distance an influence on manufactured components is given. A systematic variation of all three laser parameters is performed. A comparison of results obtained at constant energy densities obtained by varying these relevant parameters accordingly is shown as well.

1 State of the Art

1.1 Laser Sintering

Polymer Laser Sintering is an additive manufacturing process based on polymer powder. In this work an EOSINT P390 laser sintering system (EOS Company GmbH, Munich, Germany) has been used. All parts are built with a layer thickness of 150µm.
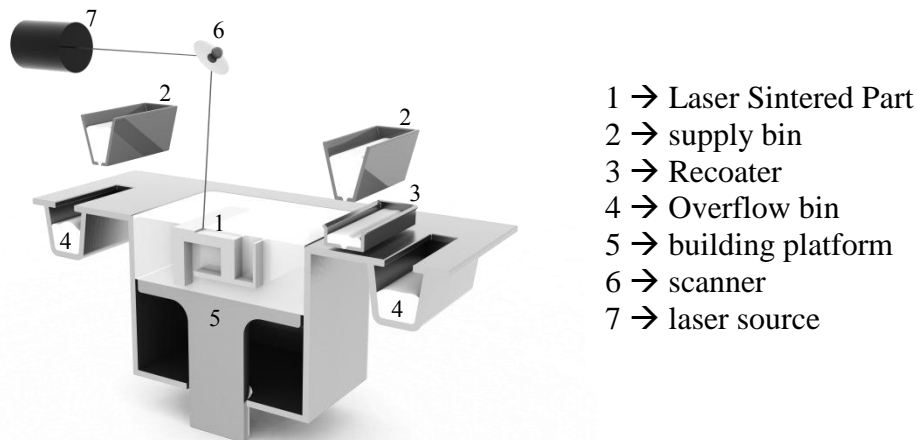
In Figure 1 a schematic representation is shown.

1 → Laser Sintered Part
2 → supply bin
3 → Recoater
4 → Overflow bin
5 → building platform
6 → scanner
7 → laser source

Figure 1: Laser Sintering Process [Ada10]

1.2 Material

Polymer Laser Sintering is a high potential additive manufacturing process. Theoretically it is possible to treat all thermoplastic materials in powder conditions [VDI3404]. Nylon 12 promises good properties as related to powder distribution, flow ability, viscosity and thermal properties to manufacture products with high requirements on strength. Approximately 80 - 90% of all laser sintered parts are produced by using nylon 12 [Sch10]. In this study, material from one batch of virgin material PA2200 (based on nylon 12) produced by EOS Company is used in order to eliminate any influence of material variations on the results. Grain shape and grain size distribution are important factors for laser sintering material and measurements are performed by a

laser diffraction method. The median value of the volume distribution is $D_{50,\,3}=55\mu m$ where the grain size distribution ranges between 30µm and 100µm.
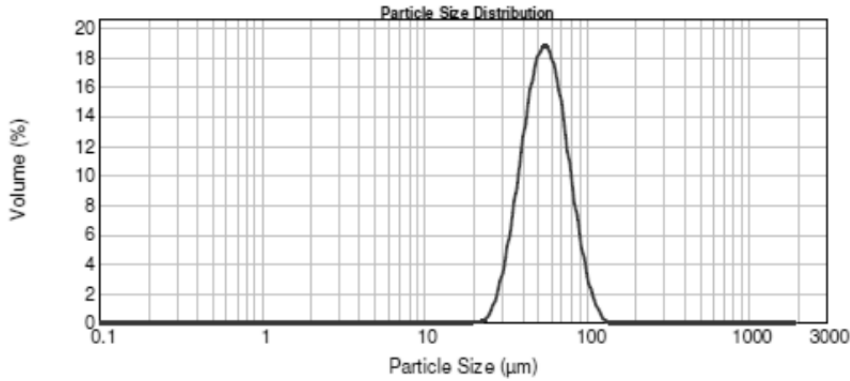

Figure 2: Volume weighted particle size distribution measured by laser diffraction

1.3 Energy Density

The laser beam contributes temporal and local energy to realize a local sintering of powder. For the determination of the energy density ED it is necessary to know the laser power P_L, the beam velocity v_B and the exposed surface A_S. According to Williams and Deckard in [WD98] the medium energy density ED_m is given by equation 1, if the intensity distribution I_L of the laser power as a function of the beam radius r_S is neglected (Figure 3):

$$ED_m = \frac{P_L}{h_S \cdot v_S} \qquad \text{(equation 1)}$$

With
ED_m = energy density,
P_L = laser power,
h_s = hatch distance,
v_s = scan velocity.
1.4 Energy Coupling

In Figure 3 a schematic description for the exposure process is shown with an intensity distribution I_L as a function of the beam diameter. In the right figure the process parameter Laser Power P_L, scan velocity v_S and layer thickness d are shown. The left figure gives information about the hatch distance h_S. The exposure vector is shown by a solid line (1). The dashed line (2) presents the *skywriting*. In this area the laser beam is run with a laser power of $L_P=0W$. With the beginning of the part, the laser power switched on with a sized value and the laser beam is running with a constant velocity.
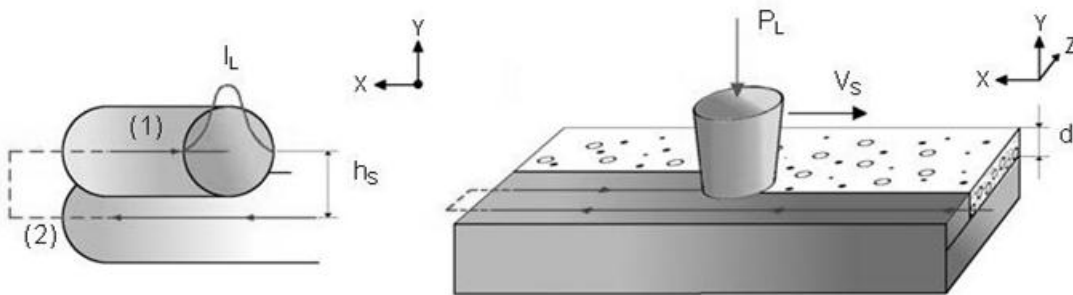

Figure 3: Schematic description for the exposure process. Left: exposure vector (1), Skywriting (2), Intensity distribution l_L as a function of beam diameter, hatch distance h_S; Right: laser power P_L, Scan velocity v_S, and layer thickness d.

The laser power P_L has an influence on the intensity of the laser beam. The hatch distance determines the overlap area and therefore the connection between two hatch lines. By increasing the laser power P_L or decreasing the scan velocity v_S, the energy density into the powder bed is increasing. Researches about the influence of energy density describe a correlation between the surface energy and part properties as strength, contour accuracy and part density. Caulfield et al. are showing a trend to more dense parts with higher values for elongation at break and tensile strength by increasing energy density [CML07]. However Sauer determines a maximum energy density [Sau05]. By increasing the energy density beyond this maximum, the strength of the part is decreasing because of a thermal damage. A similar result is given by Erdal et al. in [EDJ+09-ol]. Due to different laser sintering machines a quantitative comparison of these results is difficult. This paper is about the influence of energy density on mechanical and physical properties using a EOS EOSINT P390 Laser Sintering system. Besides the mechanical properties the main focus of this work is about physical properties like density and porosity. The influence of energy density by varying laser power, hatch distance and scanning velocity should be shown. Further on it is important to show difficulties by using different methods. A correlation between mechanical and physical properties should be verified.

2 Test Setup and Execution

This chapter describes the manufacturing of the used test specimens and the methods used for the different tests.

2.1 Tensile Tests

For the realization of the tensile tests, tensile bars in accordance with DIN 527 [DIN527] are manufactured using the laser sintering system and injection molding. The nominal dimensions can be seen in figure 3.
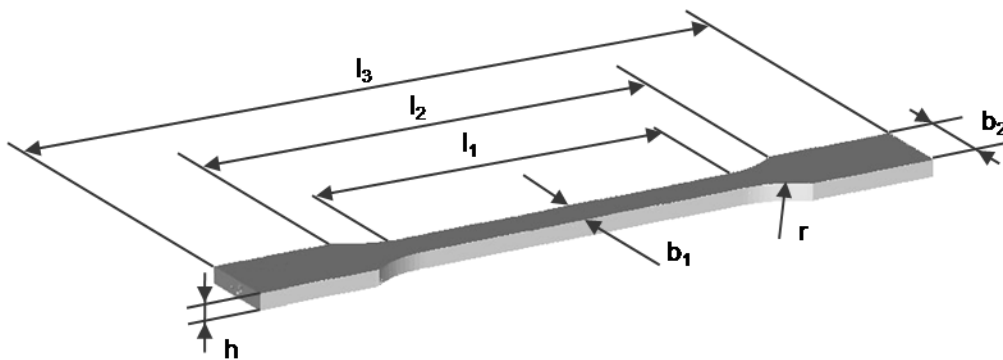

Figure 4:   Tensile Testing Bar in accordance with DIN 527

The test specimen geometry complies with the test specimen type A from Din EN ISO 3167 [DIN3167], with the following dimensions:

$b_1 = 10$ mm $h = 4$ mm
$b_2 = 20$ mm $l_1 = 80$ mm
$l_2 = 110$ mm $l_3 = 170$ mm

For tensile tests an Instron 5569 universal testing machine is used. For a determination of the Young's modulus a test speed of 1mm/min is adjusted. The test speed for the determination of tensile strength and elongation at break is 50mm/min. The elongation is detected by an *Advanced Video Extensometer*.

Using the laser sintering system, tensile testing bars oriented in X-direction as well as tensile testing bars oriented in Z-direction, are manufactured. Tensile bars in Y-direction can be excluded because of the alternating exposure strategy there are no significant changes of the part properties to be expected.
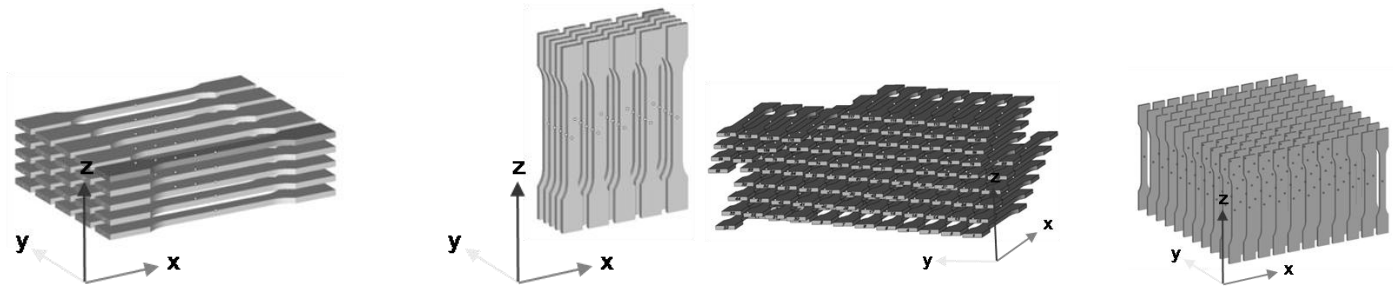
Figure 5:   Arrangement of the Tensile testing Bars in a 5x5 Matrix and 11x11 Matrix

Figure 5 shows the different orientations. Apart from the five test specimens in one plane and 5 planes on top of each other (5x5 matrix) there are also elven test specimens in one plane and eleven planes on top of each other (11x11 matrix) building jobs. Contrary to the 5x5 matrix, in build jobs with tensile testing bars oriented in X-direction of the 11x11 matrix, the tensile testing bars will be built with an offset in X-direction. This offset of the tensile testing bars in one plane shall minimize the influence of the part placement within a plane.

The arrangement of the tensile testing bars is a result of the demands in DIN 527, which requires at least the testing of five test specimens in order to determine the mechanical strength values. In order to minimize the influence of the orientation and placement within the building area, all tensile testing bars in one plane are built by using different parameters and are moved by one position in regard to the previous plane. That means that in each plane each test specimen is exposed with exactly one parameter.

Parallel to the manufacturing of test specimens using laser sintering, injection molding is used to manufacture test specimens for tensile testing in accordance with DIN 527 from PA2200.
For the manufacturing of the test specimens an ARBURG 270S injection molding machine is used, which is situated in the processing lab of the Institute for Polymer Materials (KTP). In table 1 the used parameters are listed. Before the processing a drying of the material inside a drying cabinet at T= 80°C takes place.

Table1: Parameter Settings for the Injection Molding of the Test Specimens

Adjustment			Temperature		
Parameter	Value	Unit	Tool temperature		
Dosage distance, volume	16.5	cm^3	Name	Value	Unit
Dosage speed	15	m/min	Heating unit	50	°C
Dynamic pressure	80	bar	Cooling time	25	s
Injected speed	10	cm^3/s			
Injected pressure	2,000	bar	Cylinder temperature		
Switching point follow-up pressure	6	cm^3	Name	Value	Unit
Follow-up pressure	600	bar	Adapter	40	°C
Follow-up pressure time	20	s	Heating zone 1	200	°C
Melt cushion	4.2	cm^3	Heating zone 2	210	°C
			Heating zone 3	220	°C
			Heating zone 4	220	°C
			Nozzle	220	°C

2.2 Computer Tomography

"The principle of the computer tomography consists in general of the measurement of spatial distribution of a physical property of the examined object and then calculating images without overlap from the gathered information." [Kal06]
The CT measures the weakened intensity I of the x-rays behind the measurement object. The primary intensity I_0 has to be recorded since the weakened radiation of each beam is calculated from the focus of the x-ray tube to

the receiver. The attenuation co-efficient µ can be assumed for simple cases but can only be determined by tomographic imaging for in-homogeneous objects. The projection value P (attenuation) is defined as the natural logarithm of the primary intensity I_0 to the weakened intensity I [Kal06].

The CT-Data presented within this paper have been created by the company CTM-do GmbH. The required CT data specifications for this study are met by the program VGStudio Max 2.1 from the company Volume Graphics where it is possible to conduct a defect analysis. The overall porosity of the part is determined in this process by calculating the total volume and the imperfection volume. As part of the analysis the pore size distribution of the specimen is created.

The voxel size in the current paper is about 27.6 µm x 27.6 µm x 27.6 µm. Therefore the pores volume is determined by the numbering of voxels. All volumes with a minimum volume about 8 voxels (V_{min} = 0.168-3mm^3) are detected.

2.3 Thin section cut test specimen

For thin section cuts a cuboid (figure 6) shaped test specimen with an edge length of l_K=21mm is investigated. A bar with a surface of A=8x8mm^2 and a length of l_K=21mm is extracted.
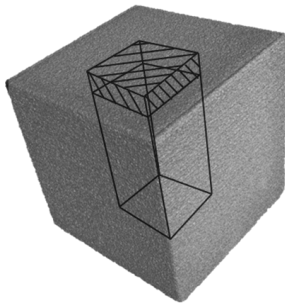

Figure 6: Cuboid to create thin section cuts

The first 2mm (shaded cuboid within the build cuboid) of the test specimen are removed to eliminate the influence of the periphery. Every thin section have a thickness of d_S=30µm, the cutting velocity is v_M=5mm/s. The hardness of the knife denoted with HK2.

The porosity ϕ_F is determined by thin section cuts and a subsequent examination using a microscope. For these experiments a *Polycut S* microtome system manufactured by Reichert-Jung company and a VHX-1 microscope (magnification: 20…200x possible) manufactured by Keyence company are used.

2.4 Test Job for the measurement of porosity and density

As a test specimen to determine the density and to use for thin section methods the cuboid explained in chapter 2.3 is used. Those cuboids are enclosed by a case to number the test specimen. The arrangement of the test specimens is shown on the right side of figure 7.
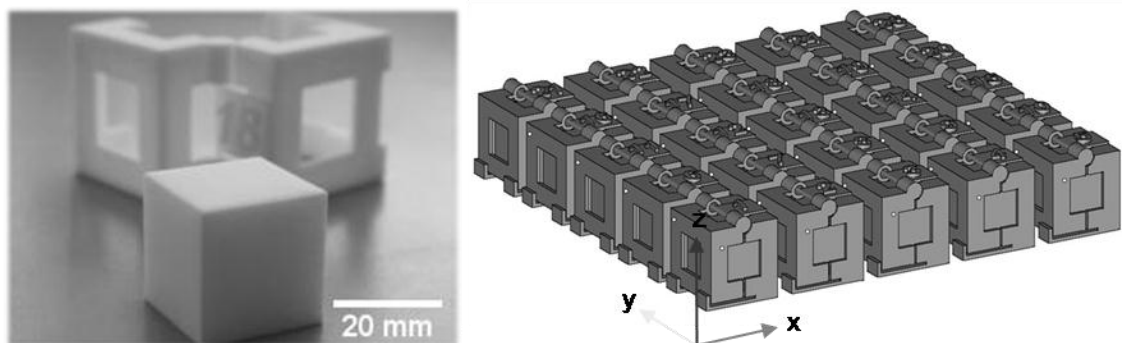

Figure 7: Test Specimens for determination of Density and creation of Thin Section Cuts

The measurement of the part density ρ_{Pr} is realized in two different ways: First, the Archimedes process is used in accordance to DIN-standard 1183 [DIN1183]. Those measurements take place in the test lab of the plastic institute of the University of Paderborn (KTP) using a scale of the type Toledo AG204 from the manufacturer METTLER TOLEDO and the needed immersion device to determine the test specimen's uplift. The weighing precision of the scale complies with the required $d_W = 0,1$ mg, according to the standard [DIN1183].

Second, the density ρ_{Pr} of the specimens is determined by pycnometry, i.e. measuring the displacement of the gas. The test specimen's weight m_{Pr} is determined. Afterwards the specimen is placed in a test chamber with a known volume. There are three different test chambers for different amounts of samples, with the volumes $V_{cell} = 8,213$ cm3, $V_{cell} = 36,589$ cm3 and $V_{cell} = 142,77$ cm3. The test chamber is filled with helium and the pressure P1 is measured. The helium then flows through a valve into expansion chamber with a known volume. The pressure P2 is measured again, with the pressure difference the volume V_{Pr} of the sample can then be determined and using the measured weight of the sample the density ρ_{Pr} can be determined as well (equation 2). The accuracy of this process is specified at +/-0.2% of the total measurement range. [MVU10] The densiy of test specimen is determined by following equation 2:

$$\rho_{Pr} = \frac{m_{Pr}}{V_{cell} - \frac{V_{Exp}}{\frac{P_1}{P_2}-1}} \qquad \text{equation 2}$$

The density measurement using a gas pycnometer is recommended for more porous structures because of the, compared to the ethanol, higher ability of the gas to fill inner porosity. Since the system is under pressure during the measurement, the filling of porous structures is supported. As part of this paper, this process is used to determine the density of the powder as well as the density of the specimen.

The density measurement using a gas pycnometer is done at the Particle Technology Group (MVU). A gas pycnometer from the manufacturer MICRMERITICS, of the type Multivolume pycnometer 1305 is used. The specimen weight is measured with a scale from the manufacturer Faust. The weighting accuracy is $d_W = 0,1$ mg.

A comparison of both methods is shown as well. The measurement of the gross density ρ_R of the used powder is done with a liquid pycnometer as well. The tests take place in the testing laboratory of the KTP in accordance with DIN standard 1183 [DIN1183]. During these test the demanded vacuum desiccator used to get rid of remaining air bubbles, is abandoned for practical reasons.

Before weighing the test material, the density ρ_{Fl} of the utilized ethanol is determined with a hydrometer. Ethanol is recommended due to its low density in order to avoid the powder from floating.
The density of the samples is determined according to equation 3:

$$\rho_{Pr} = \rho_{Fl} \cdot \frac{m_{Pr}}{m_{Fl} - m_{Pr,Fl} + m_{Pr}} \quad \text{(equation 3)}$$

With

ρ_{Pr}	density of the sample
ρ_{Fl}	density of the immersion liquid
m_{Pr}	weight of sample taken (test material)
m_{Fl}	weight of the immersion liquid
$m_{Pr,Fl}$	weight of sample taken and immersion liquid

In order to determine the sample density ρ_{Pr} , the weight of to empty as well as the weight of the completely with ethanol filled pycnometer is measured. The desired sample quantity of $m_{Pr} = 2$ g is weighed, topped up with ethanol and then weighed again. Possible remaining air bubbles are removed by swinging the container for about 10 seconds. In order to assure a reproducible filling level for all tests the intake is sealed with an inserted part. This part has a vent with a diameter of $D_E = 1$ mm, from which the excess ethanol is leaking.

3 Results and Conclusions

3.1 Density Measurement of Laser Sintered Parts

      Figure 8 plots the part densities determined with the gas pycnometer against the corresponding results of the density measurements with the Archimedes process. The difference of the results from both processes decreases with a rising energy density ED_m. The part densities determined with the gas pycnometer are higher than the ones determined with the Archimedes process. For a laser power of $P_L= 26$ W the difference is only 1% which remains this low for higher laser powers.
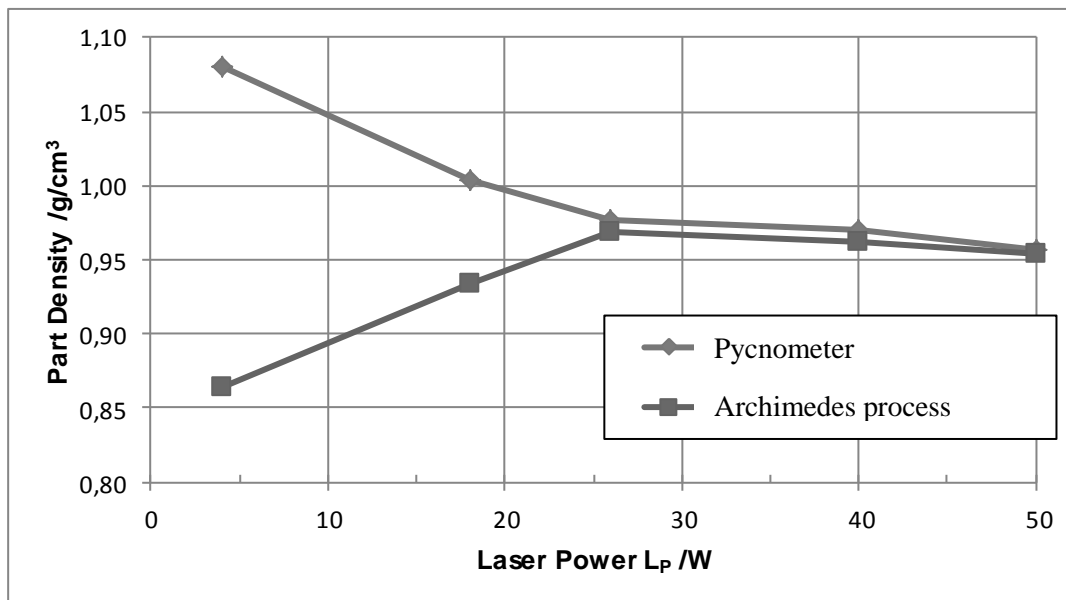

Figure 8: Comparison of the Results of the Density Measurements using the Archimedes process and the Gas Pycnometer

      The results indicate that the parts manufactured with a lower energy density show some inner porosity which can be infiltrated better by the helium compared to the ethanol. Because of that the part volume V_{Pr} is underestimated which results in a higher determined part density. Since the helium can easier infiltrate the hollows than the ethanol differences of the measured part densities occur. Because of the good match of both processes for specimens with a laser power of $P_L= 26$ W the part density seems valid. If the specimens with higher energy densities could be infiltrated a distinct difference of the results for both processes could be expected.

      The comparison of the results of the density measurements using the Archimedes process shows that the part density ρ_R decreases for an energy density below $ED_m= 33,33$ kJ/m^2 for the tensile testing bars as well as for the cuboids. Because of the uncertainties for the density measurement with the Archimedes process this has to be considered critically. It could not be detected certainly if there is in fact a decrease of 1,4% of the part density ρ_R or if it can be traced back to the measuring method. The good match of the results of the different density measurements with an energy density of $ED_m= 33,33$ kJ/m^2 and higher allows the conclusion that there are no significant changes of the part density ρ_R for an energy density of $ED_m= 33,33$ kJ/m^2 and higher.

      Because of the orientation in X- or Z- direction the energy yield varies because of the exposure vectors. The cross section to be exposed is about $A_1 = 10x4$ mm^2 for tensile testing bars oriented in Z-direction, while it is about $A_1 = 170x10$ mm^2 for tensile testing bars in X-direction. The shoulder parts of the bars are not taken into account since those are removed with a hand saw prior to the density measurement. Thus, a tensile testing bar oriented in Z-direction consists of more layers with a shorter exposure vector than a bar in X-direction.

3.2 Determination of Porosity

The results of the determination of the porosity are displayed in figure 9. It can be noticed that the porosity ϕ is between 3% and 6% for all operating points. The general underestimation of the porosity ϕ_F determined with the image analysis could be explained with the bend of the inside of the pores. Because of the chosen thickness of the section d_S the cross section of the pores A_P can be underestimated, since it decreases in the image with a higher thickness of the section. This was observed during preliminary test of the thickness of the sections d_S. For the chosen thickness of d_S= 30 µm the form of the pores could be well approximated, so that a good match of the thin section and the specimen could be expected.
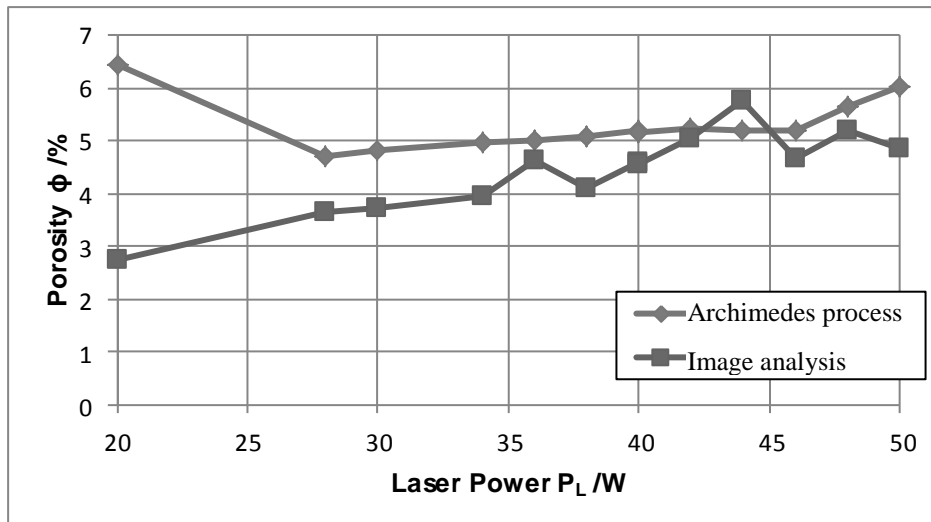

Figure 9: Comparison of the Determination of the Porosity of the Immersion Method and the Image Analysis

It is more likely that because of the image analytical determination of the porosity an underestimation of the porosity ϕ_F occurs since the border area of the specimen is not considered. The thin sections are taken from the inside of the part, the border areas seem to have a higher density though. This assumption is encouraged by the density measurement (see sections below). An increase of the porosity for a higher energy density can be observed.

3.3 The Outer Solid Area of Laser Sintered Parts

The gathered results indicate a different density on the inside and in the outer area of the part. This was confirmed by thin sections in the outer area of specimens for the density determination. A X-ray computer tomography analysis of a specimen created with an energy density of ED_m= 44,44 kJ/mm^2 shows a thick shell. The computer tomography scan was kindly provided by the company DTM-DO [CTM10]. Figure 10 shows two exemplary virtual cuts of the with the computerized tomography captured specimen. The left image shows a cut through the middle of the part, the right a cut through the part surface. It is visible that the outer area of the part has a significantly lower porosity than the inside of the part. This observation is not only obvious from the comparison of the cross sections, but from the cross section through the middle of the part alone as well. The outer area of the cross section of the middle of the part is surrounded by a shell less than 1 mm thick, which only shows a low porosity.
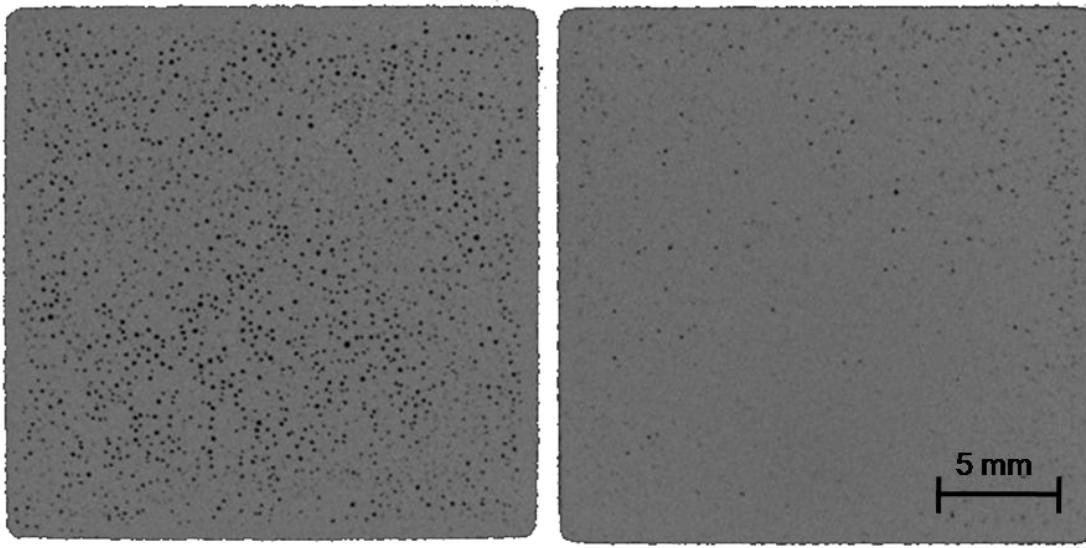
Figure 10: Virtual Cut through the Middle of th Part (left), and through the upper border of the part (right)

The dense shell encasing the specimens was also detected for specimens that were manufactured without contour- and edge-parameters. This characteristic seems to not only be a result of the contour function of the laser sintering system. There is the assumption, that the thickness of laser sintered parts as well as the cooling rate has a strong influence on the outer solid area and the porosity as well. Further experiments will examine this phenomenon.

3.4 Young's Modulus

The influence of the modulus of elasticity is shown in figure 11. In comparison the tensile testing bars created with different energy densities and in different building orientations show no significant differences in the values. The modulus of elasticity is at about $E = 2000$ N/mm^2. Therefore, only results about the elongation at break are shown.
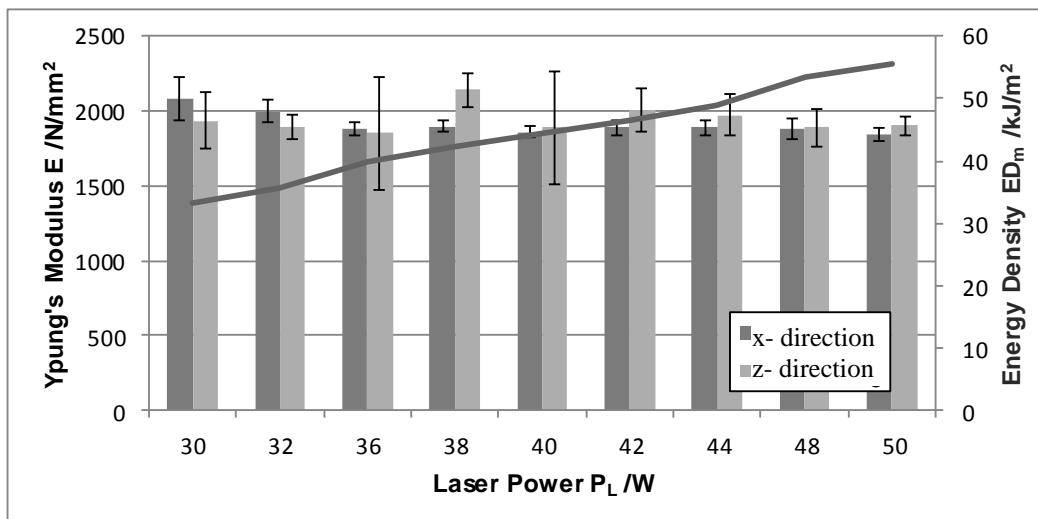

Figure 11: Modulus of Elasticity for different Energy Densities and Different Orientations

A change of the modulus of elasticity because of a variation of the building orientation or the energy density was not expected. The modulus of elasticity describes the gradient of the stress-strain-diagram in the elastic area, it is therefore primarily dependent on the used material.

3.5 Elongation at Break and Tensile Strength

In x- direction there are no differences visible. Because of this, the following results are shown for the weakest direction: z- direction.

The test series in Z-direction consisted of a job with 121 tensile testing bars (11x11 matrix) for which the energy density was varied by means of the laser power as well. During the exposure of the specimen the filling function as well as the contour function was used. The course of the stress at break of this test series is shown in figure 12.
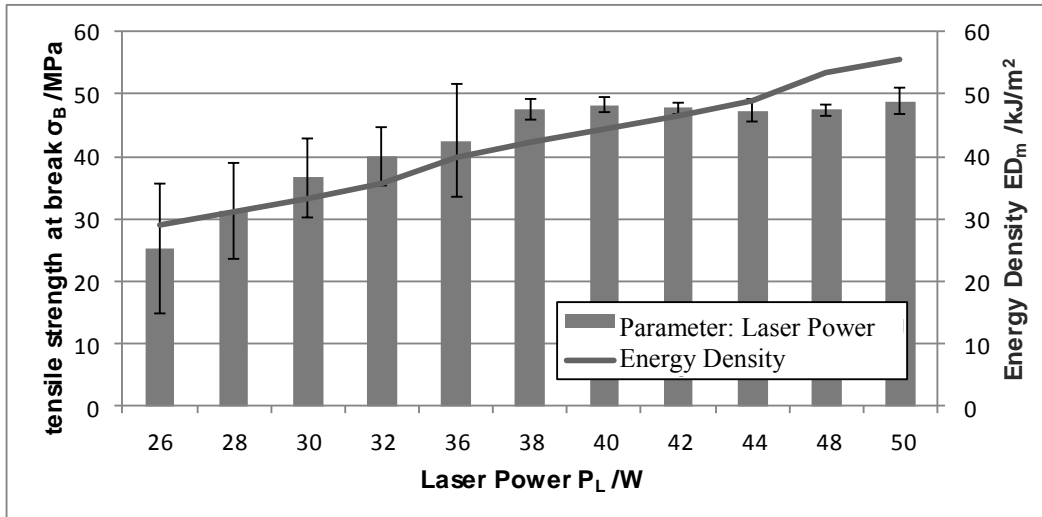

Figure 12: Tensile strength at break σ_B for varying the Energy Density ED_m with the adjusted parameter "Laser Power P_L"

With a higher energy density an increase of the average value of the stress at break can be registered as well. The recognizable trend is affected by the big spread of the Values. At an energy density of $ED_m = 42,22$ kJ/m^2 the average stress at break reaches its maximum, up to the maximum energy density of $ED_m = 55,56$ kJ/m^2 the measured stress at break is almost constant within in a range between $\sigma_B = 47,37$ MPa and $\sigma_B = 48,88$ MPa.

A similar trend can be observed for the elongation at break of the specimens in figure 13. Up to an energy density of $ED_m = 44,44$ kJ/m^2 the average value of the elongation at break increases. The spread of the values limits the significance of the average values for the elongation at break as well. A further increase of the average values of the elongation at break can be detected at an energy density of $ED_m = 53,33$ kJ/m^2, but with the biggest spread as well.
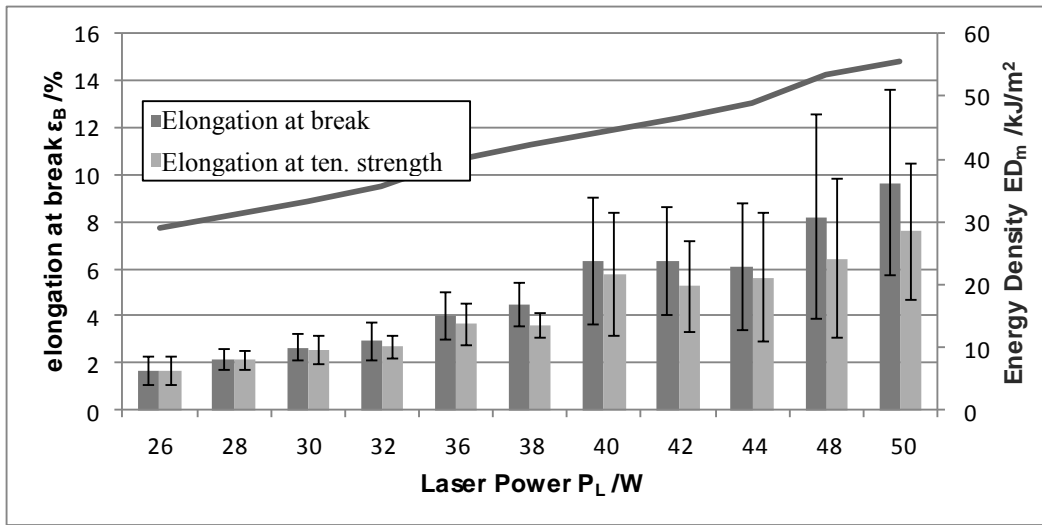
Figure 13: Elongation at break ε_B for varying the Energy Density ED_m with the adjusted parameter "Laser Power P_L"

Next, the influence of the energy density on the mechanical properties of tensile testing bars produced with different orientations is discussed. Test specimens oriented in Z-direction seems to be more influenced than tensile testing bars oriented in X-direction. A lower energy density results in a lower average value for the stress at break and a bigger spread of the single values for the stress at break for the tensile testing bars oriented in Z-direction. The elongation at break shows lower average values for lower energy densities as well, though the big spread complicates the evaluation.

Generally the maximum of the strength can be observed at an energy density of about $EDm = 44,44$ kJ/m^2, the results are not definite though. For the elongation at break a similar trend can be observed, partly high average values for the elongation at break are also achieved for higher energy densities. The spread of the values allows no final statement.

Tensile testing bars created with injection molding from PA2200 reached a slightly lower stress at break than laser sintered parts with an average value of $\sigma_B = 42,51$ MPa, but had a higher standard deviation of 6,36 MPa. A distinct difference is indicated for the achieved elongation at break of the injection molded tensile testing bars. The average was at about $\varepsilon_B = 250$ %. A parameter variation about hatch distance and scanning velocity has to be performed as well.

3.6 Tensile Bars Cross Section

The influences of the energy on the part geometry happened by considering the change of the cross section of the used tensile testing bars, which was measured prior to the tensile test for the calculation of the stress σ. The change of the specimen width b_1 is shown in figure 14, the change of the specimen thickness h in figure 15. Clearly visible is the increase of specimen cross section A_{Pr} with a higher energy density ED_m.
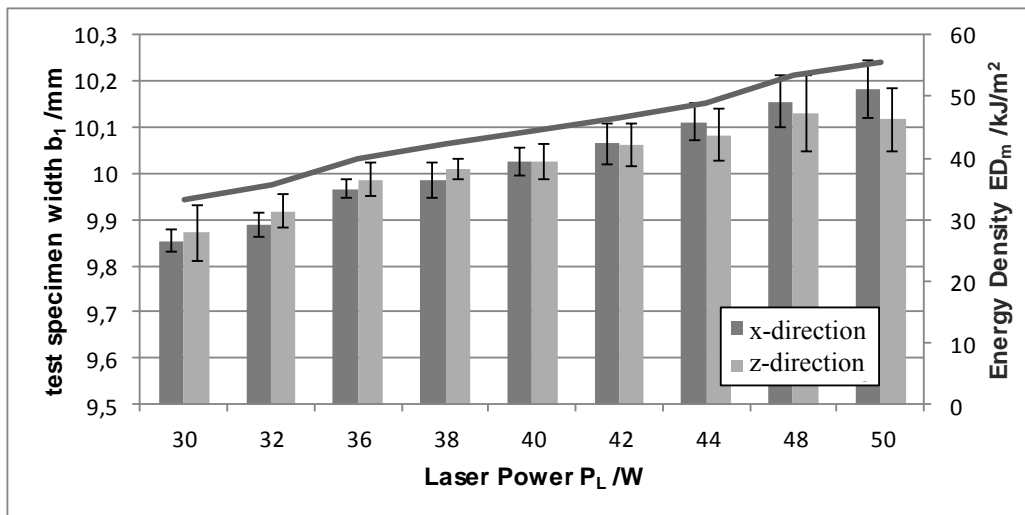
Figure 14: Measured Width of Tensile Testing Bars for different Energy Densities
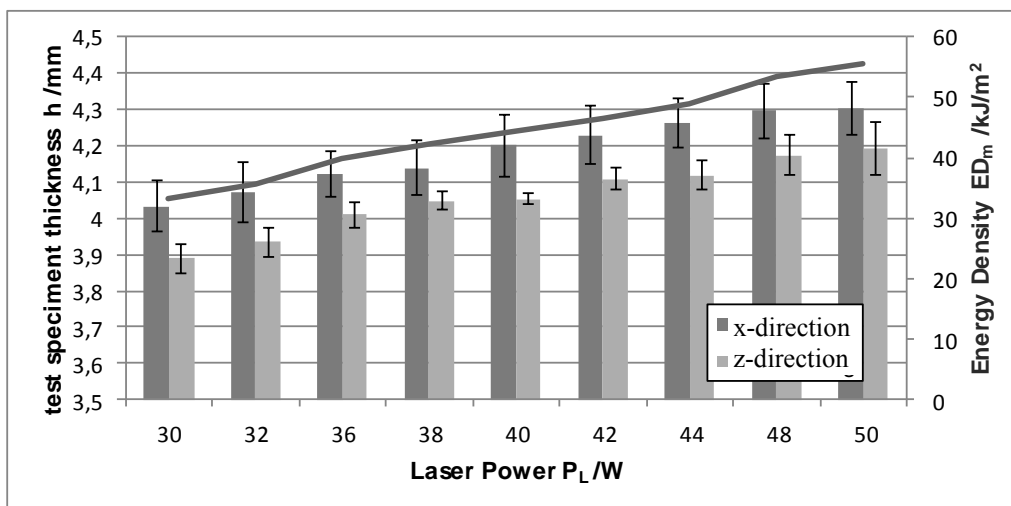

Figure 15: Measured Thickness of Tensile Testing Bars for different Energy Densities

4 Summary and Outlook

It is possible to obtain higher values for the elongation at break by using higher values for the energy densities. The maximum part density is obtained at energy densities higher than $ED_m=30kJ/m^2$. Further on an influence of energy density on the part geometry is shown as well. By increasing the energy density the cross section is increasing as well.

A summary of all results shows optimized mechanical properties for an energy density of $ED_m = 44,44$ kJ/m^2. For lower energy densities the strength in z- direction is decreased. This means, the optimum strength is obtained at energy densities which are 50% higher compared to the energy density needed to obtain maximum density. For higher energy densities it is possible to reach higher values for the elongation at break, but the material can be damaged as well by using too much energy. Further on the dimension accuracy is decreasing because of the higher heating influence zone. The results are comparable with the examinations done by Sauer [Sau05]. The results given in this paper are about a factor of 10 higher than the parameter examined by Sauer. This might be the results of different laser sintering machines. Sauer was using a Sinterstation 2000 whereas in this work an EOSINT P390 is examined. However Erdal et al. [EDJ+09-ol] determined a maximum for the energy density of $ED_m = 30kJ/m^2$, which is about 32% less than in this work.

An outer solid area is shown as well. Influencing parameters like the exposure strategy, thickness of laser sintered parts as well as cooling rate will be determined in future works. Because of the outer solid area a density measurement using the Archimedes process is sensible. The results for the part density in this work are

between $\rho_R = 0,955$ g/cm^3 and $\rho_R = 0,975$ g/cm^3. The geometry of test specimen has to be determined as well for future experiments. Further on the influence of energy density on the porosity have to be shown. It might be possible to increase mechanical properties of laser sintered parts by reducing porosity. Another influencing factor on the mechanical properties is the surface, whereby it is possible to increase it by using suitable post processing methods.

Reference

[Ada10]   Adam, G. Konstruktionsregeln für additive Fertigung in Lehre und Forschung, Berliner Kreis, Ausgabe 15, 2010, Seiten 22-23, Wirtschaftliches Forum für Produktentwickelung e.V.

[CML07]   Caulfield, B.; McHugh, P.E.; Lohfeld, S.: "Dependance of mechanical properties of polyamide components on build parameters in the SLS process"; Journal of Materials Processing Technology 182, S. 477-488; Elsevier Verlag, 2007

[CTM10]   CTM-do GmbH, Carlo-Schmid-Allee 3, 44263 Dortmund, www.CTM-do.de

[DIN1183]   DIN EN ISO 1183-1; „Kunststoffe - Verfahren zur Bestimmung der Dichte von nicht verschäumten Kunststoffen – Teil 1: Eintauchverfahren, Verfahren mit Flüssigkeitspyknometer und Titrationsverfahren" (ISO 1183-1:2004)

[DIN3167]   DIN EN ISO 3167: „Kunststoffe -Vielzweckprobekörper"; Dezember 2003

[DIN527]   DIN EN ISO 527-1 :"Kunststoffe. Bestimmung der Zugeigenschaften"; April 1996

[EDE04-ol]   Eichler, Jürgen; Dünkel, Lothar; Eppich, Bernd: "Die Strahlqualität von Lasern. Wie bestimmt man Beugungsmaßzahl und Strahldurchmesser in der Praxis?"; www.laser-journal.de; Oktober 2004, Nr. 2; Abruf: 12.02.2010; URL:
              http://onlinelibrary.wiley.com/doi/10.1002/latj.200790019/abstract

[EDJ+09-ol]   Erdal, M.; Dag, S.; Jande, Y.A.C.; Tekin, C.M.: „Production and Characterization of Uniform and Graded Porous Polyamide Structures Using Selective Laser Sintering"; Workshop on Rapid Technologies, 24.09.2009.

[Kal06]   Kalender, W.A.: Computertomographie, Publicis Corporate Publishing, 2006

[MVU10]   „Demonstrationsversuch zur Vorlesung Grundlagen der Verfahrenstechnik. Dichtebestimmung an einem Gaspycnometer der Firma Micromeritics"; 2010; Schulungsunterlagen Lehrstuhl Mechanische Verfahrenstechnik und Umweltverfahrenstechnik

[Sau05]   Sauer, Andreas: "Optimierung der Bauteileigenschaften beim Selektiven Lasersintern von Thermoplasten"; Dissertation; Shaker Verlag; 2005

[Sch10]   Schmid, Manfred: „Kunststoffe für Selektives Lasersintern"; plastics.now!; Ausgabe Juni 2010

[VDI3404]   VDI Richtlinie 3404; „Generative Fertigungsverfahren Rapid-Technologien (Rapid Prototyping) Grundlagen, Begriffe, Qualitätskenngrößen, Liefervereinbarungen", Verein Deutscher Ingenieure; Dezember 2009

[WD98]   Williams, John D.; Deckard, Carl R.: „Advances in modeling the effects of selected parameters on the SLS process"; Rapid Prototyping Journal; Volume 4, Number 2; 1998; S. 90-100; ISSN: 1355-2546
              http://www.turkcadcam.net/haber/2009/rapidtech-workshop/presentations/Presentation10.pdf